JOURNAL OF CATALYSIS 102, 386–400 (1986)

Hydrocarbon Synthesis from CO–H_2 on Supported Iron: Effect of Particle Size and Interstitials

M. A. McDONALD, D. A. STORM, AND M. BOUDART[1]

Department of Chemical Engineering, Stanford University, Stanford, California 94305

Received November 6, 1984; revised July 29, 1986

Rates of hydrocarbon synthesis (HS) from CO–H_2 (syngas) were measured for Fe supported on MgO (Fe/MgO) while Mössbauer effect spectroscopy (MES) was used for monitoring the structure of the metal. Three effects were observed as particle size d of H_2 prereduced Fe changed between 1 and 17 nm. First, the site-time yield of CH_4 synthesis (STY_{CH_4}, the number of CH_4 molecules produced per CO-titrated site per second) increased by over an order of magnitude. Second, under conditions used (525 K, $H_2/CO = 3$, atmospheric pressure), large Fe particles produced a lower fraction of C_2^+ in the hydrocarbon product (C_2^+ selectivity) and showed a greater tendency for deactivation and loss of C_2^+ selectivity than small particles. Third, as reaction in syngas proceeded, the dominant phase shifted from χ-carbide to ε'-carbide as d decreased, and further decrease of d produced a decrease in the rate of ε'-carbide formation. The three trends for HS were the same qualitatively and similar quantitatively when the catalysts were converted to ε-nitride before reaction, instead of being used directly after reduction in H_2. However, MES showed that the ε-nitride structure persisted even after 20 h in reacting syngas although measurements of CH_4 evolved during reduction of used samples indicated that the surface of all catalysts was thoroughly carbided. Thus, for HS, particle size was more important than interstitials in determining activity and selectivity of supported Fe.

INTRODUCTION

Variation of the particle size of supported metal catalysts in the range 1–10 nm can change both activity and selectivity for some reactions (*1*). The rate of hydrocarbon synthesis (HS) from CO–H_2 (syngas) on supported Fe depends on particle size, indicating that these reactions may be structure sensitive (*2*). The site-time yield for methanation (STY_{CH_4}, the number of CH_4 molecules produced per second per Fe surface atom) increased by an order of magnitude with increasing particle size of Fe supported on MgO, Fe/MgO (*3*). More recently, Jung *et al.* (*4*) found an effect of the same type and magnitude for C_1–C_6 HS on Fe/C. These particle size effects are similar to those for supported Ru, CO, and Ni (*2, 5*). However, in the case of Fe, interpretation is complicated by the conversion during HS of the initially metallic iron catalysts to carbide and by the fact that the structure of the carbide phases vary as a function of particle size (*3, 6*).

We report here the previously cited results (*3*) of the effect of particle size of initially reduced Fe/MgO on the rate of methanation from syngas. Also reported are measurements of rates of C_1–C_5 hydrocarbon synthesis in a cell which allowed Mössbauer effect spectroscopy (MES). Thus, variations in both rates of HS and structure of the interstitial iron phases could be observed as a function of iron particle size and time in reacting syngas. Chemisorption of CO and physical adsorption of N_2 were used for titration of reduced Fe surface atoms and for determination of total surface areas, respectively. Relative areas of MES metallic and oxide peaks and volumetric uptake of O_2 were used for determination of the fraction of Fe reduced.

Nitrided Fe catalysts for synthetic fuel

[1] To whom inquiries should be addressed.

0021-9517/86 $3.00

production from syngas were developed in the U.S. Bureau of Mines research program following World War II (*7–9*). These nitrided catalysts were converted to carbonitride phases during exposure to syngas. Thus, our Fe/MgO samples were also studied following nitride formation before reaction to monitor the relationship between interstitial phases and activity for HS.

EXPERIMENTAL

Catalysts were prepared as described in detail elsewhere (*3*). Magnesium oxalate was precipitated from solutions of magnesium nitrate and oxalic acid. The solid was filtered, washed, and dried in a vacuum oven. It was then slurried in water while the pH was adjusted between 9 and 10 with dilute NH_4OH. An aqueous solution of $Fe(NO_3)_3 \cdot 9H_2O$ was added dropwise while pH was maintained at 9–9.5, resulting in precipitation of Fe^{3+} on the magnesium oxalate. The solid was filtered, washed, and dried overnight at 363 K in an air oven. Different values of Fe loading were obtained by varying the molality of the $Fe(NO_3)_3 \cdot 9H_2O$ solution. The catalyst containing 0.5% Fe following reduction was prepared using a solution in which Fe was enriched in ^{57}Fe.

The catalyst precursors prepared as described above were always pretreated immediately before characterization or catalysis. This involved a dehydration in flowing O_2 for 6 h as temperature was linearly ramped from room temperature (RT) to 625 K. This was followed by a 20-h reduction in flowing H_2 at 700 K. During this latter step, the magnesium oxalate decomposed to MgO. Dioxygen (99.9%, Liquid Carbonic) was passed through a molecular sieve trap at 195 K. Dihydrogen (99.95%, Liquid Carbonic) was Pd-diffused.

All measurements of gas uptake were done in a conventional volumetric system (*10*). Adsorption of CO at 195 K was used to titrate reduced Fe surface atoms (*11*). Following reduction, a sample was cooled to 625 K in flowing H_2 and evacuated for 1.5 h to a pressure less than 1 mPa. Then the sample was cooled under vacuum to 195 K and a CO isotherm taken. Following evacuation for 600 s, a second isotherm was taken. The amount of strongly adsorbed CO was taken to be the difference between the two isotherms in the region where they were parallel (≥40 kPa) (*11*). One CO molecule was assumed to be adsorbed for every two surface Fe^0 atoms (*11*). The percentage of metallic iron exposed was thus calculated with the equation

$$\% \text{ Fe exposed} = \frac{(100)^2(2)AM_{Fe}}{Lf}. \quad (1)$$

In this equation, A is the CO adsorption in moles per g of catalyst, M_{Fe} is the molecular weight of iron, L is the weight percentage of iron in the sample (obtained from atomic absorption measurements at the Microanalysis Laboratory of the Stanford Department of Chemistry), f is the fraction of reduced iron estimated from MES spectral areas, 2 is the stoichiometry of surface Fe^0 to CO adsorbed, and the factor of $(100)^2$ arises from L and the answer being expressed as percentages. Likewise, average Fe^0 particle sizes were calculated by assuming particles were spherical, which yields the equation

$$d = \frac{6Lf10^{19}}{(0.135)\rho_{Fe}AN}. \quad (2)$$

Here, d is the average particle diameter (nm), 10^{19} is a conversion factor, ρ_{Fe} is the density of metallic iron (g cm^{-3}), N is Avogadro's number, and 0.135 is the Fe^0 surface area (nm^2) covered by one CO molecule (*11*).

Total sample areas were obtained by the BET method from adsorption of N_2 at 77 K. Fraction of Fe reduced was obtained by volumetric uptake of O_2 at 623 K. As indicated by MES (*3*), all iron was taken to be Fe^{2+} or Fe^0 before oxidation and Fe^{3+} following oxidation.

Rates of CH_4 synthesis were measured at 498, 523, and 548 K in a system previously described (*12*). Approximately 1–2 g of un-

treated catalyst were loaded into a reactor (*10*) and reduced. The catalyst was then cooled to reaction temperature in flowing H_2. A flow of CO (99.5%, Liquid Carbonic) was then added in the ratio of $H_2/CO = 3.0$ while the reactor was bypassed. When flow was established, this stream was then diverted through the reactor at space velocities between 250 and 1200 h^{-1} (volumetric gas flow per apparent catalyst volume per hour). Product samples were taken at 600-s intervals over a 2-h period with a gas sampling valve and sent to an Aerograph gas chromatograph equipped with a thermal conductivity detector. A 3-m column of Porapak Q was used to separate products. Peak areas were determined by a disk integrator on the strip chart recorder and were calibrated with a 1.03% CH_4 in He mixture (Matheson). Total CO conversion was typically less than 2%. Rate measurements at other temperatures were made in the same manner on the same samples following a 16–20 h reduction at 673 K in flowing H_2.

To measure reaction rates and obtain MES data, approximately 0.3 g of catalyst precursor was pressed into a wafer for each experiment and mounted in a cell described elsewhere (*13*). This cell was found suitable as a differential reactor free from heat or mass transfer limitations by application of the Koros–Nowak criterion (*14*). Initially reduced samples were prepared as already described, while nitride samples were prepared by 2 h treatment of the initially reduced samples in flowing NH_3 at 675 K. Following reduction or nitridation, the temperature was changed to 525 K in flows of H_2 or NH_3, respectively. When temperature stabilized, flows of H_2 and CO in the ratio $H_2/CO = 3.0$ were initiated, and in the case of nitrided catalysts, flow of NH_3 was halted. Samples of reaction products were taken by a sampling valve and sent to a Hewlett–Packard 5730A gas chromatograph equipped with a flame ionization detector. The 3 m column was filled with Porapak Q. Peak areas for the C_1–C_5 hydrocarbon products were measured with a Hewlett–Packard 3390A integrator and were calibrated with a 0.65% CH_4, 0.35% C_2H_4, 0.35% C_2H_6, 0.35% C_3H_6, and 0.35% C_3H_8 in He mixture (Matheson). The CO conversion to hydrocarbons was always less than 0.6%.

The gas chromatograph was also used to determine the amounts of carbon-containing species accumulated on the catalysts during reaction. These were obtained from plots of STY_{CH_4} obtained during reduction of used catalysts at 675 K in H_2 versus the time of treatment in H_2, which could be integrated and multiplied by the surface Fe/total Fe ratio to give CH_4/Fe values for each sample. Only a small amount of C_2H_4 and C_2H_6 were produced in addition to the CH_4 evolved.

Dihydrogen (99.95%, Liquid Carbonic) and carbon monoxide (99.8%, Matheson) were passed through molecular sieve traps at 195 K before use. Ammonia (99.99% "Anhydrous," Matheson) was passed through a molecular sieve trap at RT before use.

The Mössbauer effect spectrometer is described elsewhere (*15*). The source was 100 mCi of Co^{57} in Pd and the symmetric constant acceleration drive waveform was used. All isomer shifts are referenced to a 12-μm Fe foil. Spectra were fitted using the computer program described elsewhere (*16*). All spectra were taken at RT, and unless otherwise noted, were cooled to RT in a flow of the same gas used during collection of the subsequent spectrum.

RESULTS

The CO adsorption data and N_2 BET areas for the series of samples are shown in Table 1. The fraction of Fe reduced estimated from either MES peak areas or from O_2 uptake, also shown, increased with increasing Fe loading as is typical for Fe/MgO (*17*). The CO adsorption measurements indicate Fe exposed decreased from 100% at low values of Fe loading to about 6% at the highest values (5–10% Fe). This

TABLE 1

Characterization of Initially Reduced Fe/MgO

% Fe	CO uptake (μmol g^{-1})	Fraction Fe reduced		Percentage of Fe^0 exposed	Iron particle size (nm)	BET area (m^2 g^{-1})
		From MES	From O_2 uptake			
10	51.7	0.90	—	6.6	16	235
4.6	24.3	0.92	—	6.3	17	—
2.1	22.5	0.66	0.85	18	5.9	—
1.1	26.0	0.61	—	43	3.0	—
0.7	17.1	—	—	61	—	281
0.6	14.9	—	0.76	62	2.3	—
0.5	20[a]	0.40	—	100	1.5	310
0.4	18.9	—	—	—	—	—
0.2	21.5	—	—	—	—	—

[a] Determined with less precision (± 2 μmol g^{-1}) than adsorptions on other samples (± 0.4 μmol g^{-1}); experimental problems prevented a precise determination of CO uptake on this sample.

corresponds to average particle sizes ranging from 1 to 17 nm over the same range. The BET area decreased with increasing Fe loading, as observed for Fe/MgO prepared by other methods (*18*).

The rate of methane formation is reported as STY_{CH_4}, site-time yield, i.e., number of molecules of CH_4 produced per exposed Fe^0 atom per second. The values of STY_{CH_4} at 523 K, atmospheric pressure, and $H_2/CO = 3.0$ (Table 2) increased by an order of magnitude as particle size increased. Apparent activation energies showed no trend with respect to particle size.

Measurements of the STY of C_1–C_4 hydrocarbon synthesis made using the MES cell are shown in Figs. 1 and 2. The two catalysts used, 10 and 0.5% Fe/MgO, had 6 and 100% Fe exposed, respectively. The initial STY for CH_4 synthesis is essentially equal to that shown in Table 2 for samples with the same % Fe exposed (Table 3). The smaller particles had marginally better activity maintenance over a 20-h period, although both samples showed substantial

TABLE 2

Site-Time Yield: CH_4 Synthesis on Initially Reduced Fe/MgO

% Fe	Percentage of Fe^0 exposed	% CO conversion	Space velocity (h^{-1})	STY_{CH_4} (10^{-4} s^{-1})	E_{app} (kJ mol^{-1})
4.6	6.3	0.8	1200	39.0	—
—		2.0	462	34.0	128
2.1	18	0.9	600	10.0	118
—		1.5	300	16.0	—
1.1	43	0.3	333	3.3	135
—		0.2	429	4.0	—
0.6	62	0.2	261	1.9	141
0.4	100	0.1	600	2.7	132
0.2	100	0.1	462	2.2	—

Note. $H_2/CO = 3.0$, atmospheric P, 523 K, 600 s of reaction.

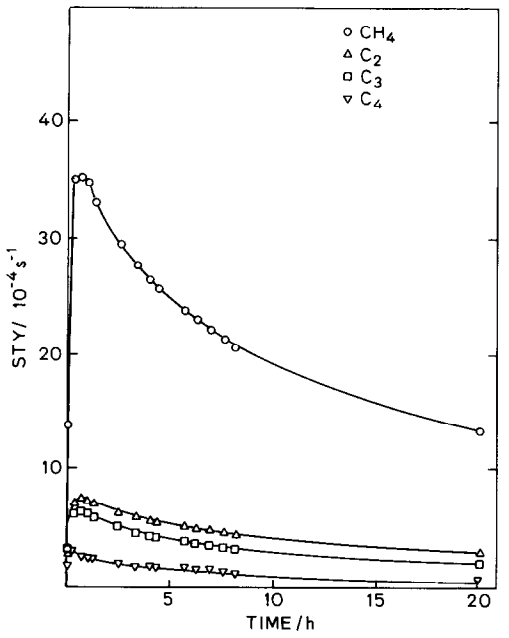

FIG 1. The STY for hydrocarbon synthesis on initially reduced 10% Fe/MgO from $H_2/CO = 3$ at 525 K and atmospheric pressure, versus time on stream.

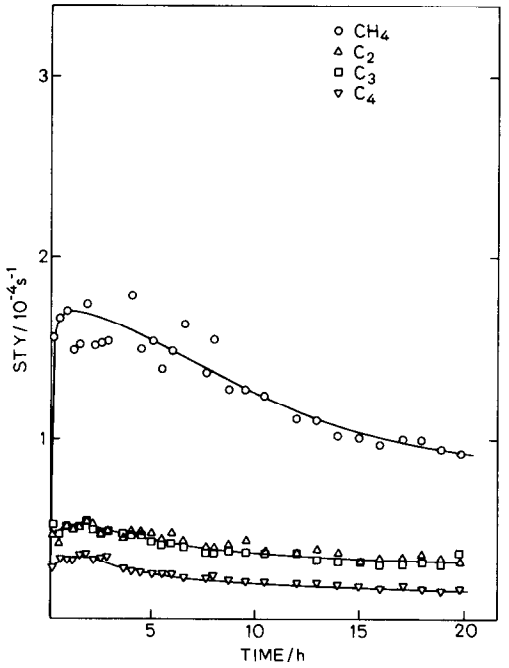

FIG. 2. The STY for hydrocarbon synthesis on initially reduced 0.5% Fe/MgO from $H_2/CO = 3$ at 525 K and atmospheric pressure, versus time on stream.

TABLE 3

$CO-H_2$ Reactions on Fe/MgO

% Fe	Initial composition	Time on stream (h)	STY_{CH_4} (10^{-4} s^{-1})	C_4/CH_4
10	Reduced	0.5	36	0.085
		20	14	0.037
0.5	Reduced	0.5	1.7	0.19
		20	0.94	0.18
10	Nitride	0.5	85	0.10
		20	45	0.065
0.5	Nitride	0.5	2.5	0.16
		20	1.5	0.14

deactivation. The smaller particles also showed both better selectivity and better maintenance of selectivity to C_2^+ hydrocarbons, as seen from the C_4/CH_4 ratios in Table 3. This can also be seen from Fig. 3, the "Anderson–Schulz–Flory" plot (*19, 20*), in which the rate of C_1–C_5 production is normalized with respect to the rate of CH_4 production for both catalysts with time of reaction as the varied parameter. The 0.5% Fe catalyst produced a higher C_2^+ fraction

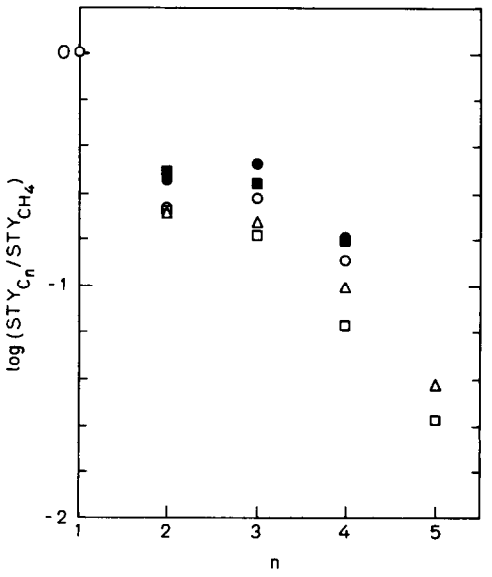

FIG. 3. "Anderson–Schulz–Flory" plot for initially reduced Fe/MgO. Logarithm of ratio STY's versus carbon number *n*. The conditions are those of Figs. 1 and 2. 10% Fe/MgO: (○) 0.1 h, (△) 0.4 h, (□) 6.3 h. 0.5% Fe/MgO: (●) 0.5 h, (■) 6.0 h.

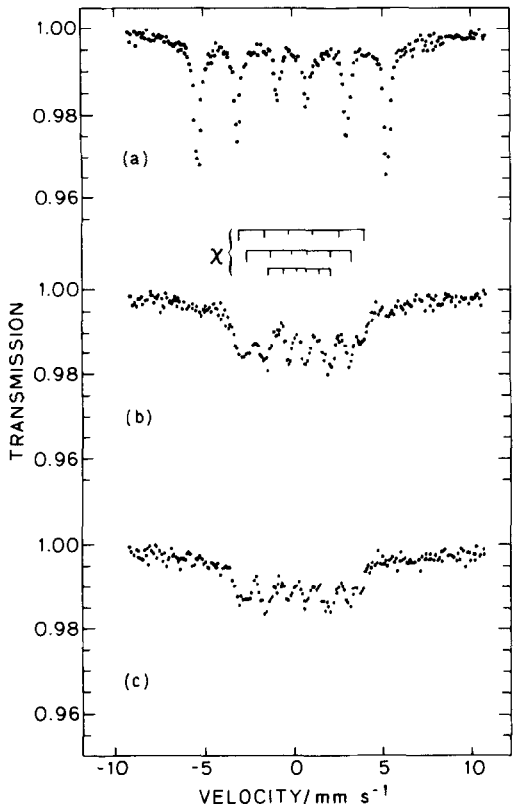

FIG. 4. MES of 10% Fe/MgO at room temperature. (a) Initially reduced catalyst, in flowing H_2. (b) Reduced catalyst treated in $H_2/CO = 3$ for 2 h at 525 K, in flowing He. (c) Reduced catalyst treated in $H_2/CO = 3$ for 20 h at 525 K, in flowing He.

initially and this fraction was relatively unaffected by time on stream. In contrast, the 10% Fe catalyst produced a lower initial C_2^+ fraction and the C_2^+ fraction decreased with time, as selectivity shifted toward CH_4 production.

Small particles of Fe also formed a higher fraction of olefins in the C_2^+ product, in agreement with other work (*4*). For small particles, the fraction of ethylene in the C_2 product was two to four times higher than for large particles. However, the large particle catalyst was much more active than small particles of Fe, so % CO conversion was 10–20 times higher. Since secondary hydrogenation of olefins produced during HS depends strongly on % CO conversion (*4*), these results suggest trends, but are not conclusive.

The MES of the two catalysts after reaction, shown in Figs. 4 and 5, also differ substantially. Figure 4a shows the spectrum of initially reduced 10% Fe/MgO, in which the six-peak spectrum characteristic of α-Fe is visible as well as traces of the Fe^{2+} doublet with isomer shift of about 1 mm s^{-1}. Previous studies of Fe supported on MgO have shown that this component is due to Fe^{2+} substituted for Mg^{2+} in the MgO phase, forming an $(Fe^{2+}, Mg^{2+})O$ support for Fe^0 particles (*11, 18*). Figure 4b, taken after 2 h of reaction, shows only traces of zerovalent Fe remaining, as most of this iron was con-

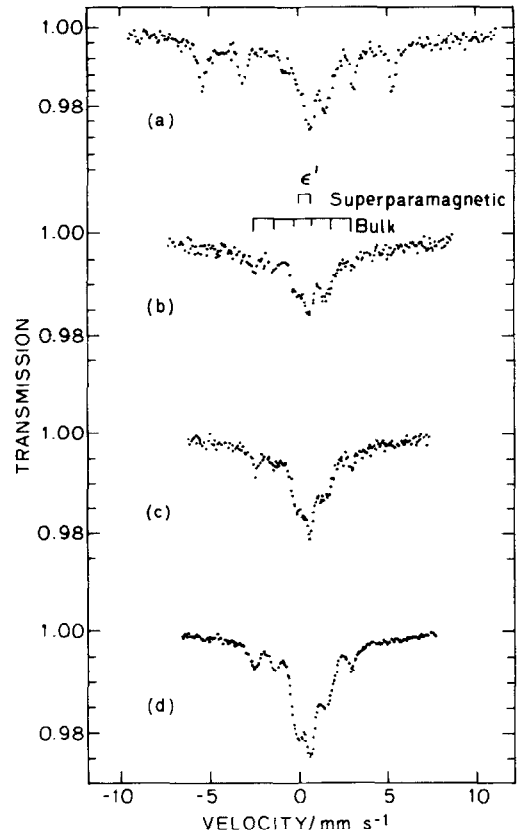

FIG. 5. MES of 0.5% Fe/MgO at room temperature and flowing H_2. Heating and cooling of reacted samples done in flowing He. (a) Intially reduced catalyst, in flowing H_2. (b) Reduced catalyst treated in $H_2/CO = 3$ for 2 h at 525 K. (c) Sample in (b) after 20 h total in $H_2/CO = 3$ at 525 K. (d) Sample in (c) after 42 h total in $H_2/CO = 3$ at 525 K.

TABLE 4

MES Parameters of 0.5% Fe/MgO

Figure	Component	Fraction	Width (mm s^{-1})	Isomer shift[a] (mm s^{-1})	Quadrupole splitting (mm s^{-1})	H (kOe)
5b	ε′	0.32	0.55	0.26	—	172
	SP-ε′	0.20	0.47	0.27	0.87	—
	Fe^{2+}	0.48	0.74	0.96	1.07	—
5c	ε′	0.24	0.42	0.29	—	166
	SP-ε′	0.35	0.62	0.28	0.81	—
	Fe^{2+}	0.41	0.83	0.94	1.00	—
5d	ε′	0.25	0.49	0.26	—	170
	SP-ε′	0.40	0.62	0.31	0.81	—
	Fe^{2+}	0.35	0.81	0.95	1.11	—
11a	ε-Nitride	0.74	0.59	0.40	0.32	—
	Fe^{2+}	0.26	0.45	1.09	0.83	—
11b	SP-Carbonitride	0.19	0.24	0.24	0.66	—
	Fe^{2+}	0.81	0.74	1.05	0.95	—
11c	Carbonitride	0.46	0.86	0.26	—	158
	Sp-carbonitride	0.20	0.62	0.25	0.52	—
	Fe^{2+}	0.34	0.56	1.08	0.88	—

[a] With respect to α-Fe at room temperature.

verted to carbide as seen by peaks in the center of the spectrum. Most of this carbide spectrum can be attributed to the monoclinic χ-carbide (*21, 22*), although some peaks due to the hexagonal close-packed phase usually referred to as ε′-carbide may also be present (*22, 23*). Although there is considerable disagreement in the literature concerning the correct assignments for MES of iron carbides (*6, 22, 24*) because of their numerous overlapping peaks, the assignments made here are adequate for qualitative identification of carbide phases present. The spectrum in Fig. 4c (the sample for which STY data are shown in Fig. 1) is predominantly that of χ-carbide, with no bulk Fe^0 remaining.

The 0.5% FE/MgO sample gave quite different MES data. The spectrum of the reduced catalyst in Fig. 5a shows the six-peak spectrum of metallic iron and a doublet due to Fe^{2+}. The doublet is broadened toward the lower-velocity side, and this is attributed to superparamagnetic Fe^0 (*8*). The computer fitting for these spectra is shown in Table 4.

Figure 5b shows the spectrum of 0.5% Fe/MgO taken after 2 h of reaction. The magnetically split Fe^0 component disappeared and was replaced by a six-peak component due to hexagonal close-packed ε′-carbide. A doublet due to superparamagnetic ε′-carbide also developed during reaction (*23*). The Fe^{2+} doublet was relatively unaffected by reaction. Due to the strong amount of overlap between Fe^{2+} and superparamagnetic ε′-carbide, their MES parameters in Table 4 are not very precise. Subsequent reaction in syngas of the same sample gave new results (Figs. 5c and d). The intensities of the bulk ε′-carbide and Fe^{2+} doublet were relatively unaffected, but the superparamagnetic ε′-carbide component increased in intensity with reaction time in syngas. This can be seen in Fig. 6, in which the intensities of the carbide components are plotted as a function of time on stream. These intensities are all normalized with respect to Fe^{2+} intensity, since adjustments in the electronics of MES data collection made the absolute intensities vary from spectrum to spectrum.

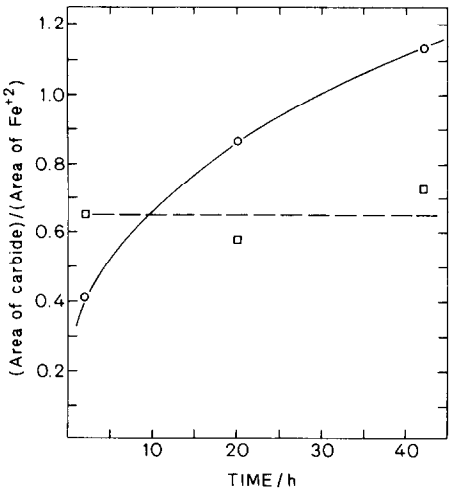

FIG. 6. Ratios of MES spectral areas in Fig. 5 versus time. (○) (Area superparamagnetic ε′)/(Area Fe^{2+}); (□) (Area bulk ε′)/(Area Fe^{2+}).

The STY for hydrocarbon synthesis on the two initially nitrided catalysts is shown in Figs. 7 and 8 as a function of time. The STY is somewhat higher than for the reduced catalysts, particularly for the 10% Fe/MgO sample. The selectivity patterns (Fig. 9) were about the same as for the reduced catalysts except for a short induction period on nitrided 0.5% Fe/MgO during which the fraction of CH_4 was higher than on the reduced catalyst. The 0.5% Fe/MgO sample showed better maintenance of activity and selectivity to C_2^+ hydrocarbons, just as for the reduced catalysts. The rates and selectivity data for initially reduced and nitrided catalysts are summarized in Table 3.

The Mössbauer effect spectrum of initially nitrided 10% Fe/MgO shown in Fig. 10a is a paramagnetic doublet. After 2 h of reaction, the spectrum (Fig. 10b) shows a distribution of magnetic splittings. The sepctrum appears to be composed of the paramagnetic component and at least two other broad components with magnetic fields averaging 110–140 and 200–240 kG. After 20 h of reaction, two six-peak components with magnetic fields averaging 148

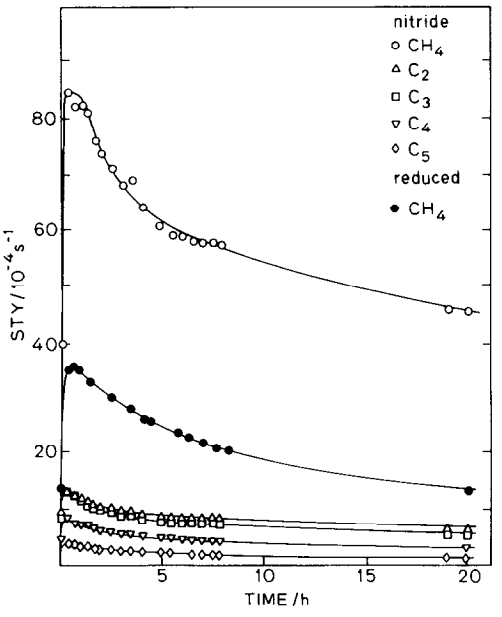

FIG. 7. The STY for hydrocarbon synthesis on initially nitrided 10% Fe/MgO from $H_2/CO = 3$ at 525 K and atmospheric pressure, versus time on stream. The STY for CH_4 synthesis on the initially reduced catalyst (Fig. 1) is shown for the purpose of comparison.

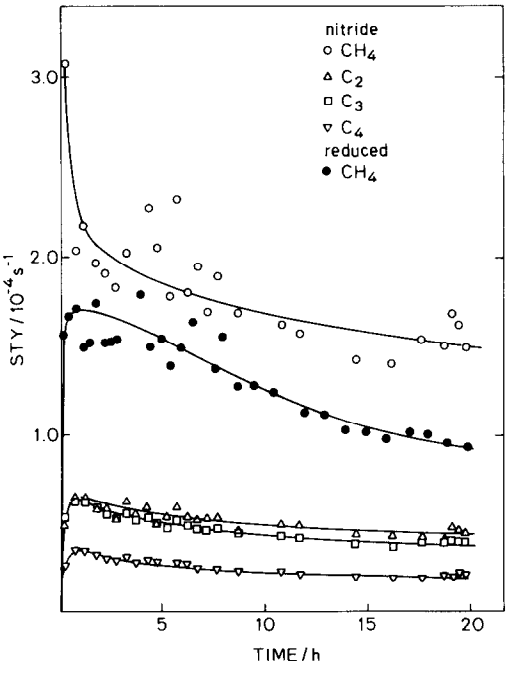

FIG. 8. The STY of hydrocarbon synthesis on initially nitrided 0.5% Fe/MgO from $H_2/CO = 3$ at 525 K and atmospheric pressure, versus time on stream. The STY for CH_4 synthesis on the initially reduced catalyst (Fig. 2) is shown for the purpose of comparison.

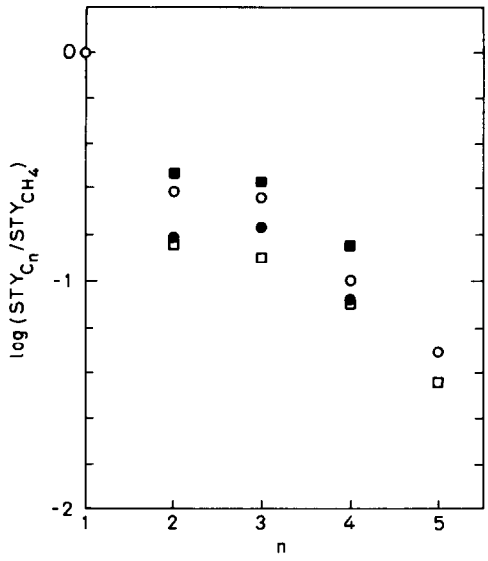

FIG. 9. Anderson–Schulz–Flory plot for initially nitrided Fe/MgO. 10% Fe/MgO: (○) 0.1 h, (□) 6.0 h. 0.5% Fe/MgO: (●) 0.2 h, (■) 0.6 h.

and 230 kG are clearly visible, and the paramagnetic component has apparently disappeared (Fig. 10c). A trace of a component with magnetic field of approximately 300 kG may also be present.

The spectra in Fig. 10 indicate that the iron phase in the 10% Fe/MgO was paramagnetic ε-nitride or ζ-nitride before reaction and was mainly ε-nitride even after 20 h of reaction (*25, 26*). The disappearance of the paramagnetic component and the increased intensity of the magnetically split components was due to a loss of N atoms from the nitride lattice during reaction (*26*).

This interpretation is consistent with what is known about the structure and MES of iron nitrides. The ε-nitride phase has a hexagonal close-packed lattice of Fe atoms with N occupying the interstitial octahedral sites, and is isostructural with ε′-carbide (*7*). Unlike other iron nitride phases, ε-Fe_xN has a broad composition range with $2 < x < 3.2$ (*7*). Three different magnetically split components have been observed in the Mössbauer effect spectra of ε-nitride. These components (qualitatively indicated in Fig. 10) have average magnetic fields equal to or less than 300, 240, and 150 kG, and have been attributed to Fe atoms with one, two, or three N atoms as neighbors, respectively (*25, 26*). Thus, for an ε-nitride with the minimum amount of N in the lattice, each Fe atom would be expected to have only one or two N neighbors, consistent with the two six-peak components observed with $H = 298$ kG and 238 kG (*27*). Samples of ε-nitride with slightly more N in the lattice would be expected to have Fe atoms with either two or three atoms as neighbors, and thus show spectra qualitatively similar to Fig. 10c (*26, 28*). It should be noted here that both the average magnetic field of each of these components apparently increases slightly as %N decreases (*16*) and the linewidths of those magnetically split peaks are much broader than the natural linewidths. Both of these facts seem to be due to the presence of a distribution in hyperfine fields for atoms

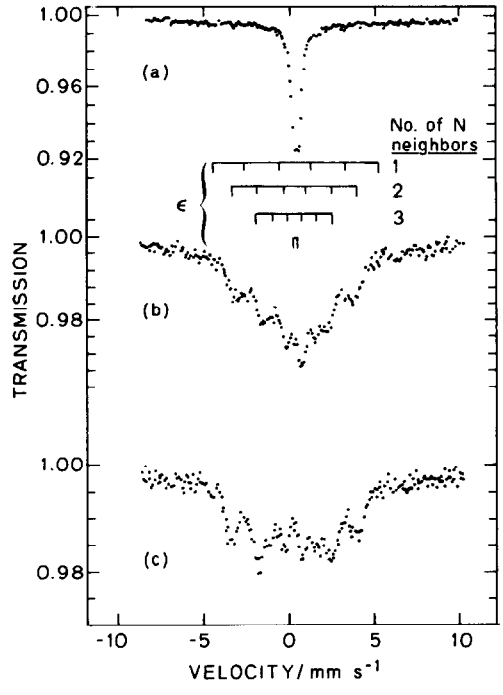

FIG. 10. MES of 10% Fe/MgO at room temperature. (a) Reduced catalyst treated in NH_3 for 2 h at 675 K, spectrum in flowing NH_3. (b) Nitride treated in $H_2/CO = 3$ for 20 h at 525 K, spectrum in flowing He. (c) Sample in (a) treated in $H_2/CO = 3$ for 20 h at 525 K, spectrum in flowing He.

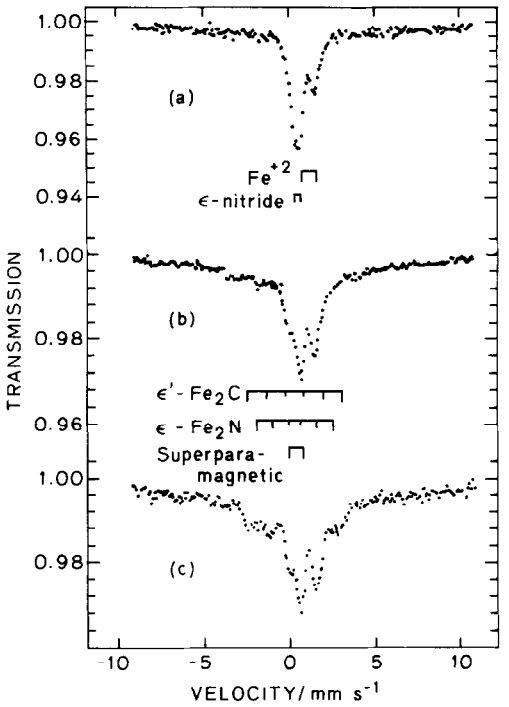

FIG. 11. MES of 0.5% Fe/MgO at room temperature. (a) Reduced catalyst treated in NH_3 for 2 h at 675 K, spectrum in flowing NH_3. (b) Sample in (a) treated in $H_2/CO = 3$ for 2 h at 525 K, spectrum in flowing He. (c) Nitride treated in $H_2/CO = 3$ for 20 h at 525 K, spectrum in flowing He.

with a given number of nearest neighbor N; although the hyperfine field at an Fe^{57} nucleus depends mainly on how many nearest neighbor N it has, it also depends on the distribution of N at longer distances.

However, the Curie temperature of Fe_xN also decreases as x increases, and is below RT for an x of 2.3–2.5 or lower (*25, 26, 28*). Therefore, Fig. 10a is either ε-Fe_xN ($x < 2.5$) or possibly ζ-nitride, which has a similar spectrum and a composition Fe_2N; either assignment is consistent with the isomer shifts and quadrupole splittings observed (*26, 29*), and only low temperature MES can distinguish the two compounds. Since such a distinction is unnecessary for the purpose of this work, the doublet will henceforth be called "paramagnetic ε-nitride." During the initial 2 h of reaction, N was lost from the lattice, and, as will be shown later, the surface regions of the nitride particles were carburized, resulting in the magnetically split components in Fig. 10b. This process continued during longer times of reaction, yielding the spectrum in Fig. 10c, which is similar to that of ε-$Fe_{2.67}N$ reported elsewhere (*26*). Although a carbide spectrum may also be present among the overlapping peaks in Figs. 10b and c, it is clear that the spectra are mainly ε-nitride and that this assignment is sufficient for qualitative identification of the composition.

The spectrum of initially nitrided 0.5% Fe/MgO in Fig. 11a shows the same paramagnetic ε-nitride doublet overlapping with the Fe^{2+} doublet. After 2 h of reaction (Fig. 11b), a doublet similar to that of superparamagnetic ε'-carbide developed, and traces of magnetically-split components also developed, while the paramagnetic nitride component decreased in intensity and the Fe^{2+} doublet was unaffected. The spectrum taken after 20 h of reaction (Fig. 11c) shows a magnetically split component with very broad peak widths. These broad widths appear to be due to a distribution of magnetic fields for the absorber atoms. The magnetic fields range between those expected for Fe atoms in ε'-carbide (*22, 23*) and Fe atoms in ε-nitride with three N neighbors (*26*) (approximate positions of both components are indicated in Fig. 11). Thus, the magnetically split component can best be described as an ε-carbonitride phase. The superparamagnetic doublet can also be considered to be an ε-carbonitride phase, although its parameters listed in Table 3 are quite similar to superparamagnetic ε'-carbide. This is consistent with the idea that N should be most thoroughly removed from the smallest particles in the particle size distribution. The Fe^{2+} doublet was relatively unaffected.

The loss of subsurface N during reaction is consistent with carburization of the surface regions of iron nitride particles during reaction. The degree of carburization of initially reduced and nitrided catalysts is summarized in Table 5 as ratios of CH_4 molecules produced during reduction of reacted catalysts per Fe atom (CH_4/Fe). The degree

TABLE 5

Reduction of Used Catalysts (675 K) in H_2

% Fe	Initial state	Time of reaction (h)	Ratio of the total number of CH_4 molecules produced per Fe atom (CH_4/Fe)
10	Reduced	2	0.50
		20	0.65
	Nitride	20	0.65
0.5	Reduced	2	1.11
		20	2.13
	Nitride	20	2.08

of carbon buildup obviously increased with time of reaction for all samples. For initially reduced 10% Fe/MgO, the CH_4/Fe ratio increased substantially after 20 h of reaction compared to the value obtained after 2 h, even though MES of the catalysts after 2 h of reaction showed almost no metallic Fe. Although the c/Fe ratio in carbide phases is somewhat uncertain, it is ≤ 0.5 (*25*). Since nearly all the CH_4/Fe ratios are greater than this upper limit, the difference must be due to surface carbonaceous material (carbidic carbon, graphitic carbon, adsorbed CO, and growing hydrocarbon chains). The increase in CH_4/Fe ratio with time of reaction indicates that the amount of surface carbonaceous material increases with time, which correlates with decreased activity and selectivity to C_2^+ hydrocarbons.

The extent of surface carbonaceous deposits is clearer for 0.5% Fe/MgO, particularly when it is considered that much of the iron in this sample is oxidized and therefore not carburized. The smaller iron particles on this catalyst had a higher fraction of Fe exposed, and thus higher CH_4/Fe ratios in Table 5, since a higher fraction of the CH_4 produced during reduction must come from surface carbon. After accounting for subsurface C and unreduced Fe, the two initially reduced catalysts had CH_4/Fe ratios equivalent to several monolayers of carbonaceous material on the iron surface after 20 h of reaction.

The initially nitrided catalysts showed CH_4/Fe ratios not substantially lower than those for initially reduced catalysts, even though MES clearly showed that the subsurface iron in the working catalyst was not thoroughly carburized. Thus, the surface of the nitrided catalyst is essentially as extensively carburized as the reduced catalysts during reaction.

DISCUSSION

Particle Size Effect on Rates of Hydrocarbon Synthesis (HS)

The results in Table 1 demonstrate that average iron particle size increased with increasing % Fe. It is possible that the calculated Fe particle sizes could be underestimated due to an overestimation of CO adsorption, since Topsøe *et al.* (*30*) concluded that Fe/MgO samples adsorbed CO on the support oxide as well as on the reduced Fe. However, any CO adsorption on the support in the amounts they reported would not substantially alter the magnitude of the particle size effect on STY. Furthermore, MES of the 0.5% Fe/MgO sample showed an average iron crystallite size substantially less than 3 nm, consistent with the particle size of 1.5 nm in Table 1 (*13*). Thus, our particle sizes are reliable for present purposes.

The effects of Fe particle size on HS are quite similar to those reported by Jung *et al.* (*4*). They found that for carbon-supported Fe, the STY_{CH_4} was over an order of magnitude greater on large (>20 nm) particles than on small (ca. 2 nm) particles. Furthermore, smaller particles produced a lower fraction of CH_4 in the hydrocarbon product, just as for Fe/MgO. The Fe/carbon catalysts also showed similar trends in activity maintenance; at 508 K, the value of STY_{CH_4} on the large-particle catalyst decreased by a factor of 2 over a 45-h period, while for the small-particle catalyst, the value of STY_{CH_4} was essentially constant over the same time period. These trends agree qualitatively with those for Fe/MgO and would be expected to be in better quantitative agreement if measured at the same temperature.

Although the magnitude of the particle size effect on activity and selectivity on Fe/MgO agrees with that found with other catalysts, the values of STY_{CH_4} are lower than those reported elsewhere. Jung *et al.* (*4*) reported STY_{CH_4} values which were 3–10 times those for Fe/MgO catalysts of the same particle size, and Vannice (*31, 32*) found that large particles of Fe on Al_2O_3 or SiO_2 had STY_{CH_4} exceeding those for large particles of Fe on MgO by the same magnitude.

At least part of this disagreement may reflect the fact that techniques used for titration of surface Fe in these studies differed from those presented here for Fe/MgO. Most of these studies used CO or H_2 adsorption on used catalysts to titrate surface Fe. Since carbonaceous deposits left on the surface reaction would tend to reduce the amount of Co or H_2 adsorbed relative to the amount adsorbed on the freshly reduced catalyst, the STY reported would tend to be higher than if based on adsorption on fresh catalysts. In addition, the definition of the amount of strongly adsorbed CO, and, in some cases, the assumed CO : surface Fe ratio and the temperature of the measurement, were different from that used for Fe/MgO. Finally, rates of reaction in most of these studies were not measured under steady exposure to syngas, but were measured during cyclical exposure to syngas followed by exposure to H_2, then to syngas, etc. The effect of periodic exposures to H_2 may also be to increase rates measured and thus the STY reported. The net effect of all these factors is to lower the values of STY_{CH_4} reported by factors of 2–5 when corrected to the conditions used here while not substantially changing the magnitude of the particle size effect for Fe/carbon. In support of this, the value of STY_{CH_4} measured for large particles of Fe on SiO_2 during continuous exposure to syngas and based on estimates of surface Fe on fresh catalysts (*23, 33*) agree within a factor of 2 with results for large particles of Fe on MgO. Thus, the values of STY_{CH_4} reported for an iron catalyst of a given particle size agree at least within a factor of 3 regardless of support.

A comparison of the STY measured on initially nitrided catalysts with those for initially reduced catalysts indicates that bulk iron composition has a relatively small effect. The value of STY_{CH_4} on initially nitrided catalysts was somewhat higher than on initially reduced catalysts, but the increase was only a factor of 2 or less. In contrast, the magnitude of the particle size effect on STY_{CH_4}, selectivity, and maintenance of activity and selectivity were all essentially the same. Furthermore, except for the initial induction period, the difference in values of STY_{CH_4} between initially nitrided and reduced catalysts was constant with time on stream, even though MES has shown that with increased time on stream N atoms were lost from the bulk while catalysts were extensively carburized, particularly at the surface. Thus, if nitride catalysts were intrinsically more active, one would expect that differences in values of STY_{CH_4} would disappear as the nitride was carburized.

Therefore, for hydrocarbon synthesis on supported iron, particle size appears to be the primary factor determining activity and selectivity while support, preparation method, or bulk composition have a secondary effect at best. What differences in activity exist between initially nitrided and reduced large Fe particles can be attributed to differences in the surface carbide which develops in syngas on catalysts either initially reduced or nitrided. The higher activity of initially nitrided catalysts can be rationalized in terms of the results of Biloen *et al.* (*34*). They found that during hydrocarbon synthesis on Ru, Co, or Ni, there was a low surface coverage of active intermediates leading to CH_4 and C_2^+ products while most of the surface was covered with a relatively inactive carbonaceous "overlayer." Thus, initially nitrided catalysts may simply have a higher surface coverage of active intermediates than do initially re-

duced catalysts; however, in either case the surface coverage of active intermediates is low. This is consistent with what is known about CO adsorption on Fe and other transition metals. Dissociation of CO, which proceeds rapidly even at RT on large Fe particles (*35*), is generally considered to be the initial step in both the carburization of bulk Fe and in catalytic hydrocarbon synthesis (*22, 23, 36*). An inspection of the trends shows that transition metals which most rapidly dissociate CO (e.g., Fe, Mo) (*37*) also form bulk carbides in syngas atmospheres, whereas those which do not dissociate CO or do so only at reaction temperature (Pt, Pd, Ir, Ni, Ru) do not form bulk carbides during reaction.

Thus, the overwhelming tendency for the dissociation of CO on Fe can be considered to be at least partially due to a thermodynamic driving force for bulk carburization. The initial presence of a bulk interstitial nitride or carbide may therefore be expected to moderate the rate of CO dissociation. Thus, a lower fraction of the surface is covered by polymeric or inactive carbidic carbon while a larger number of surface sites are active for hydrocarbon synthesis. A similar trend has been observed for Mo on Al_2O_3. Initially metallic Mo on Al_2O_3 had a lower STY_{CH_4} than the same catalyst which was carburized before reaction (*38*).

The particle size effect on rates of catalytic reactions cannot be ascribed to a particle size effect on rates of deactivating side reactions (*39*). Indeed, the value of the STY for HS increased with particle size, but so did the tendency for deactivation and loss of C_2^+ selectivity. Thus, the magnitude of the particle size effect on STY may tend to be a lower limit, and may be even larger when measured under conditions less favorable for deactivation due to deposition of carbonaceous material. This is consistent with the idea that structure sensitivity is less likely to be observed when the catalyst surface is extensively covered with carbonaceous material, since differences in surface structure of the catalyst would be minimized under these conditions (*2*).

Effects of Particle Size on Bulk Composition

The effect of iron particle size on the nature of the carbide phase formed during syngas reaction is quite consistent with that reported by others. For initially reduced Fe supported on MgO, SiO_2 (*6*), or carbon (*40*), the χ-carbide phase disappeared as particle size decreased, and the ε'-carbide became the predominant phase. The lack of dependence of this trend on the nature of the support used suggests that this trend is predominantly due to a particle size effect, not to Fe–support interactions.

The superparamagnetic ε'-carbide component in MES is due to the smaller particles in the particle size distribution while the magnetically split component is due to the larger particles in this distribution. Thus, the data in Fig. 6 suggest that the conversion of iron to ε'-carbide became slower as particle size decreased, and that the rate of carburization to ε' therefore decreases with particle size. However, a comparison with other work indicates that the dependence of the carbide phase formed (ε' or χ) on particle size may also be due to similar kinetic factors. Niemantsverdriet *et al.* (*22*) found that for large particles of Fe, the ε'-carbide was favored over the χ-carbide at either lower temperature or shorter times in syngas while the χ-carbide predominated at higher temperature or long times in syngas. Thus, the effect of increasing particle size on rate of carbide formation and carbide phase formed appears to be analogous to the effects of increasing time or temperature, and may therefore be due to similar kinetic factors.

CONCLUSIONS

The STY of hydrocarbon synthesis increased over an order of magnitude as particle size of Fe supported on MgO was increased from 1 to 17 nm. Selectivity to C_2^+

hydrocarbons decreased as Fe particle size increased, however. Furthermore, maintenance of activity and C_2^+ selectivity also decreased as particle size was increased.

These trends did not depend on the nature of the interstitial phases present in the iron catalysts during use. Furthermore, the same trends have been observed by others for Fe on other supports (*4*).

The effect of iron particle size on carbide phase formed was similar to that reported for Fe supported on SiO_2 or carbon (*6, 40*). The effect of increasing particle size on carbide formation is similar to the effects of increasing time or temperature of exposure to syngas, and may be due to similar kinetic factors.

Thus, iron particle size appears to be a dominating factor in determining activity and selectivity of supported Fe for hydrocarbon synthesis. Although additional work remains in elucidating the kinetic step or steps in the reaction sequence responsible for this particle size effect, the results of this work are consistent with hydrocarbon synthesis on Fe being at least moderately structure sensitive. Indeed, our MES data as well as constant values of the activation energy do not reveal a significant interaction between metal and support, so that a change in catalytic activity and selectivity with particle size may be ascribed to changes in surface structure, as postulated for ammonia synthesis on similar Fe/MgO catalysts (*29, 41, 42*) and subsequently confirmed by large single crystal studies (*43*).

ACKNOWLEDGMENTS

This work was supported by National Science Foundation Grant NSF CPE 8219066 and earlier NSF grants. The help of Professor Ray Everson is gratefully acknowledged.

REFERENCES

1. Boudart, M., *in* "Proceedings, 6th International Congress on Catalysis, London, 1976" (G. C. Bond, P. B. Wells, and F. C. Tompkins, Eds.), Vol. I, pp. 1–9. The Chemical Society of London, 1977.
2. Boudart, M., and McDonald, M. A., *J. Phys. Chem.* **88,** 2185 (1984).
3. Storm, D. A., Ph.D. dissertation. Stanford University, 1978.
4. Jung, H-J., Walker, P. L., Jr., and Vannice, M. A., *J. Catal.* **75,** 416 (1982).
5. Reuel, R. C., and Bartholomew, C. H., *J. Catal.* **85,** 78 (1984).
6. Raupp, G. B., and Delgass, W. N., *J. Catal.* **58,** 348 (1979).
7. Anderson, R. B., *in* "Advances in Catalysis and Related Subjects" (W. G. Frankenburg, V. I. Komarewsky, and E. K. Rideal, Eds.), Vol. 5, p. 355. Academic Press, New York, 1953.
8. Anderson, R. B., *Catal. Rev.-Sci. Eng.* **21,** 53 (1980).
9. Borghard, W. G., and Bennett, C. O., *Ind. Eng. Chem. Prod. Res. Dev.* **18,** 18 (1979).
10. Hanson, F. V., Ph.D. dissertation. Stanford University, 1974.
11. Boudart, M., Delbouille, A., Dumesic, J. A., Khammouma, S., and Topsøe, H., *J. Catal.* **37,** 486 (1975).
12. Iglesia, E., and Boudart, M., *J. Catal.* **81,** 214 (1983).
13. McDonald, M. A., Ph.D. dissertation. Stanford University, 1983.
14. Madon, R. J., and Boudart, M., *Ind. Eng. Chem. Fundam.* **21,** 438 (1982).
15. Topsøe, H., Ph.D. dissertation. Stanford University, 1972.
16. Borghard, W. S., Ph.D. dissertation. Stanford University, 1981.
17. Topsøe, H., Dumesic, J. A., and Mørup, S., "Applications of Mössbauer Spectroscopy" (R. Cohen, R., Ed.), Vol. 2, p. 55. Academic Press, New York, 1980.
18. Topsøe, H., Dumesic, J. A., Derouane, E. G., Clausen, B. S., Mørup, S., Villadsen, J., and Topsøe, N., *in* "Preparation of Catalysts, II" (B. Delmon, P. Grange, P. Jacobs, and G. Poncelet, Eds.), p. 365. Elsevier, Amsterdam, 1979.
19. Anderson, R. B., *J. Catal.* **55,** 114 (1978).
20. Madon, R. J., *J. Catal.* **57,** 183 (1979).
21. Bernas, H., Campbell, I. A., and Fruchart, R., *J. Phys. Chem. Solids* **28,** 17 (1967).
22. Niemantsverdriet, J. W., van der Kraan, A. M., van Dijk, W. L., and van der Baan, H. S., *J. Phys. Chem.* **84,** 3363 (1980).
23. Amelse, J. A., Butt, J. B., and Schwartz, L. H., *J. Phys. Chem.* **82,** 558 (1978).
24. Le Caër, G., Dubois, J. M., Pijolat, M., Perrichon, V., and Bussiere, P., *J. Phys. Chem.* **86,** 4799 (1982).
25. Ron, M., "Applications of Mössbauer Spectroscopy" (R. Cohen, Ed.), Vol. 2, p. 329. Academic Press, New York, 1980.
26. Chen, G. M., Jaggi, N. K., Butt, J. B., Yeh, E. B.,

and Schwartz, L. H., *J. Phys. Chem.* **87,** 5326 (1983).
27. Eickel, K. H., and Pitsch, W., *Phys. Status Solidi* **39,** 121 (1970).
28. Mekata, M., Yoshimura, H., and Takati, H., *J. Phys. Soc. Japan* **33,** 62 (1972).
29. Bainbridge, J., Channing, D. A., Whitlow, W. H., and Pendlebury, R. E., *J. Phys. Chem. Solids* **34,** 1579 (1973).
30. Topsøe, H., Topsøe, N., Bohlbro, H., and Dumesic, J. A., *in* "Proceedings, 7th International Congress on Catalysis, Tokyo, 1980" (T. Seiyama and K. Tanabe, Eds.), p. 247. Elsevier, Amsterdam, 1981.
31. Vannice, M. A., *J. Catal.* **37,** 449 (1975).
32. Vannice, M. A., *J. Catal.* **50,** 228 (1977).
33. Amelse, J. A., Schwartz, L. H., and Butt, J. B., *J. Catal.* **72,** 95 (1981).
34. Biloen, P., Helle, J. N ., van den Berg, F. G. A., and Sachtler, W. M. H., *J. Catal.* **81,** 450 (1983).
35. Kishi, K., and Roberts, M. W., *J. Chem. Soc. Faraday Trans. 1* **71,** 1715 (1975).
36. Unmuth, E. E., Schwartz, L. H., and Butt, J. B., *J. Catal.* **63,** 404 (1980).
37. Brodén, G., Rhodin, T. N., Brucker, C., Benbow, R., and Hurych, Z., *Surf. Sci.* **59,** 593 (1976).
38. Boudart, M., Lee, J. S., and Locatelli, S., submitted for publication.
39. Boudart, M., and Cheng, W.-C., submitted for publication.
40. Jung, H.-J., Vannice, M. A., Mulay, L. N., Stanfield, R. M., and Delgass, W.N., *J. Catal.* **76,** 208 (1982).
41. Dumesic, J. A., Topsøe, H., Khammouma, S., and Boudart, M., *J. Catal.* **37,** 503 (1975).
42. Dumesic, J. A., Topsøe, H., and Boudart, M., *J. Catal.* **37,** 513 (1975).
43. Spencer, N. D., Schoonmaker, R. C., and Somorjai, G. A., *J. Catal.* **74,** 129 (1982).